

Anisotropic magnetic properties and tunable conductivity in two-dimensional layered NaCrX₂ (X=Te,Se,S) single crystals

Jiale Huang,¹ Bingxian Shi,¹ Feihao Pan,¹ Jinchen Wang,¹ Juanjuan Liu,¹ Daye Xu,¹ Hongxia Zhang,¹ Tianlong Xia,¹ and Peng Cheng^{1,*}

¹*Laboratory for Neutron Scattering and Beijing Key Laboratory of Optoelectronic Functional Materials and MicroNano Devices, Department of Physics, Renmin University of China, Beijing 100872, China*

Monolayer NaCrX₂ (X=Te,Se,S) were theoretically proposed to be two-dimensional intrinsic ferromagnetic semiconductors while their physical properties have not been thoroughly investigated in bulk single crystals. We report the single-crystal growth, structural, magnetic and electronic transport properties of NaCr(Te_{1-x}Se_x)₂ ($0 \leq x \leq 1$) and NaCrS₂. For NaCr(Te_{1-x}Se_x)₂, the strong perpendicular magnetic anisotropy of NaCrTe₂ can be gradually tuned to be a nearly isotropic one by Se-doping. Meanwhile, a systematic change in the conductivity with increasing x is observed, displaying a doping-induced metal-insulator-like transition. Under magnetic field larger than 30 kOe, both NaCrTe₂ and NaCrSe₂ can be polarized to a ferromagnetic state. While for NaCrS₂, robust antiferromagnetism is observed up to 70 kOe and two field-induced metamagnetic transitions are identified along H||ab. These intriguing properties together with the potential to be exfoliated down to few-layer thickness make NaCrX₂ (X=Te,Se,S) promising for exploring spintronic applications.

INTRODUCTION

Magnetism in two dimensions has been a fascinating topic in condensed matter physics for decades. From the initial investigations on thin-film magnets to the recent discovery of two-dimensional (2D) magnetic order in ultra-thin van der Waals (vdW) materials, a wide range of possibilities for both spintronic applications and fundamental research have been opened up[1–3]. For few-layer vdW crystals, 2D magnetism has been realized in metallic Fe₃GeTe₂[4, 5], semiconducting CrI₃/Gr₂Ge₂Te₆[6, 7] and insulating FePS₃[8, 9] due to the large magnetic anisotropy which could counteract thermal fluctuations. These materials can serve as different building blocks of vdW heterostructures depending on their conductivity and exploring potential applications in novel magneto-electronic devices. Therefore magnetic anisotropy and conductivity are two key properties of 2D magnetic materials. Finding new 2D materials and ways to tune these properties would be quite important in the research of 2D magnetism.

Bulk CrTe₂ with 1T phase is a vdW ferromagnet with in-plane magnetic anisotropy and Curie temperature of 310 K[10]. Remarkably, in untra-thin flakes or films, the easy axis of CrTe₂ changes from in-plane to out-of-plane and room-temperature ferromagnetism is retained[11–14]. Moreover, a recent study identified a zigzag type antiferromagnetic order in monolayer CrTe₂[15], demonstrating the intricacy of 2D magnetism in this material. On the other hand, the intercalations of metal atoms into the vdW gap of CrX₂ (X=Te,Se,S) can form plenty of new phases. Although the structures of these intercalated CrTe₂ phases are non-vdW type, many of them are still able to be exfoliated into nanosheets while keep intriguing physical properties. For example, the room-temperature ferromagnetism in 10 nm-thick Cr-intercalated CrTe₂[16]

and the superionic behavior in 1.1 nm-thick AgCrS₂[17] have been reported recently. Especially for the latter, the structure of so-called AgCrS₂ monolayer consists of one Ag layer sandwiched between two [CrS₂] layers with actual formula AgCr₂S₄, which has been shown to be stable experimentally[17].

The Na-intercalated NaCrX₂ (X=Te,Se,S) are recently proposed to be a class of monolayer ferromagnetic semiconductors by first-principles calculations[18]. Although the crystal structures are non-vdW type, their cleavage energies are comparable with other 2D materials. It also should be mentioned that, in previous research the vdW magnetic material CrTe₂ is mainly made by deintercalating the alkali metal of KCrTe₂. However the physical properties of NaCrTe₂ have not been thoroughly investigated until recently. Experimentally, NaCrTe₂ is determined to be an A-type antiferromagnet with T_N=110 K and perpendicular magnetic anisotropy[19, 20]. With applied magnetic field, spin-flip-driven giant negative and angle-dependent magnetoresistance are observed for single crystals of NaCrTe₂[20]. For NaCrSe₂ and NaCrS₂, although their antiferromagnetic transition temperature and structure have already been determined[21], the anisotropic and field-induced magnetic properties are still unclear due to the lack of single crystals. Furthermore, chemical doping has been proved to be an effective way to tune the magnetic and transport properties of layered magnetic materials[22–25]. It would be interesting to explore the Se-doping effect on NaCrTe₂.

In this paper, we report the successful growth of single crystals of NaCr(Te_{1-x}Se_x)₂ and NaCrS₂. These crystals show intriguing magnetic and transport properties, including field-induced spin-flip transitions, giant negative magnetoresistance, chemical doping controlled magnetic anisotropy and conductivity. Our findings suggest the NaCrX₂ series are promising candidates for further

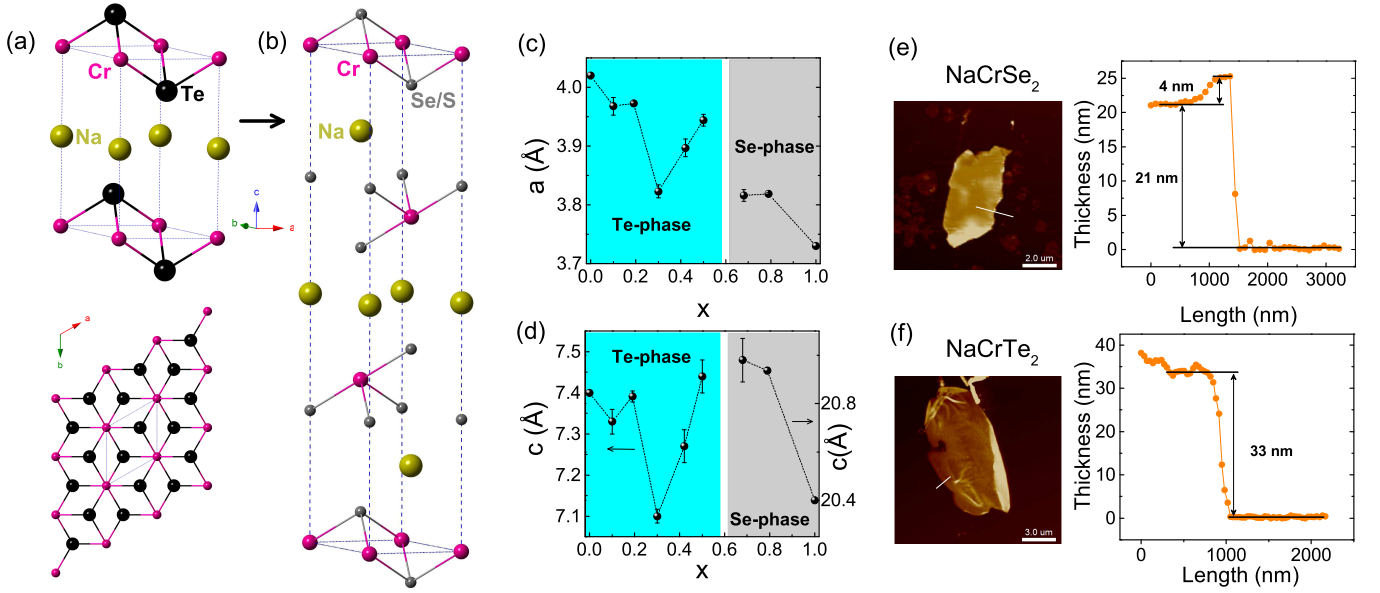


FIG. 1. (a) Crystal structure of NaCrTe₂ (up) and top view (down) of CrTe₂ layer. The blue dotted lines represent the unit cell. (b) Crystal structure of NaCrSe₂ and NaCrS₂. (c,d) Lattice parameters obtained by fitting single crystal x-ray diffraction data for NaCr(Te_{1-x}Se_x)₂. (e,f) Atomic force microscopy images and height profile step of NaCrSe₂ and NaCrTe₂ nano-flakes mechanically-exfoliated onto a 300 nm SiO₂/Si substrate.

investigations in 2D limit.

METHODS

Single crystals of NaCr(Te_{1-x}Se_x)₂ and NaCrS₂ were grown by melting stoichiometric elements. High-purity Na, Cr, Te and Se/S were mixed in the mole ratio 1:1:2(1-*x*):2*x*. These reagents were mixed in alumina crucibles and sealed into an evacuated quartz tube. The assembly was heated up to 1050 °C and maintained at this temperature for 24 h. Then it was slow-cooled to 800 °C at a rate of 3 °C/h and annealed at this temperature for one day before furnace-cooled to room temperature. In order to make the reaction adequate, before heating to 1050 °C, the assembly would stay for ten hours at the temperatures slightly below the melting or boiling point of each reactant. The plane size of the obtained NaCr(Te_{1-x}Se_x)₂ single crystals is up to 6 mm×6 mm, while the size of NaCrS₂ is smaller which is typically 1 mm×1 mm. NaCrTe₂ is air-sensitive, its shining surface could be oxidized and discolored after being put in the air for a few hours. With Se-doping, the crystal become less air-sensitive and it takes about two days for NaCrSe₂ to become degenerative in the air. NaCrS₂ is air-stable.

We characterized all samples with energy dispersive x-ray spectroscopy (EDS, Oxford X-Max 50). For NaCr(Te_{1-x}Se_x)₂ with *x*=0.1 and *x*=0.2, the EDS value is quite close to the nominal value. For *x*>0.3, the doping concentration may slightly deviate from the nominal

value (the estimated error is about 20%). In order to be accurate, all measured samples have been carefully checked by EDS. The descriptions in this paper about doping level *x* all refer to the EDS values.

X-ray diffraction (XRD) of the samples were collected from a Bruker D8 Advance X-ray diffractometer and a Bruker D8 VENTURE single-crystal diffractometer using Cu K_α radiation. Magnetization and electrical transport measurements were carried out in Quantum Design MPMS3 and PPMS-14T, respectively. The dimensions of exfoliated NaCrTe₂ and NaCrSe₂ nanoflakes were checked by a Bruker edge dimension atomic force microscope.

RESULTS AND DISCUSSIONS

Crystal structure of NaCrX₂

As shown in Fig. 1(a) and confirmed by XRD analysis, NaCrX₂ crystallizes in a hexagonal structure with the space group of *P*-3*m*1 for X=Te and *R*-3*m* for X=Se/S, same as previous reports[19–21]. The crystal structure of NaCrTe₂ can be considered as the intercalation of Na atoms between 1T-CrTe₂ layers. Na and Cr atoms stack alternately along the *c*-axis in the same site. The Cr atoms form a triangular lattice in the *ab*-plane. When Te was substituted by Se or S, the major change in crystal structure is the interlayer stacking order. Comparing with NaCrTe₂, for NaCrSe₂ and NaCrS₂, both Na- and Cr-triangular lattice layers are stacked along the *c*-

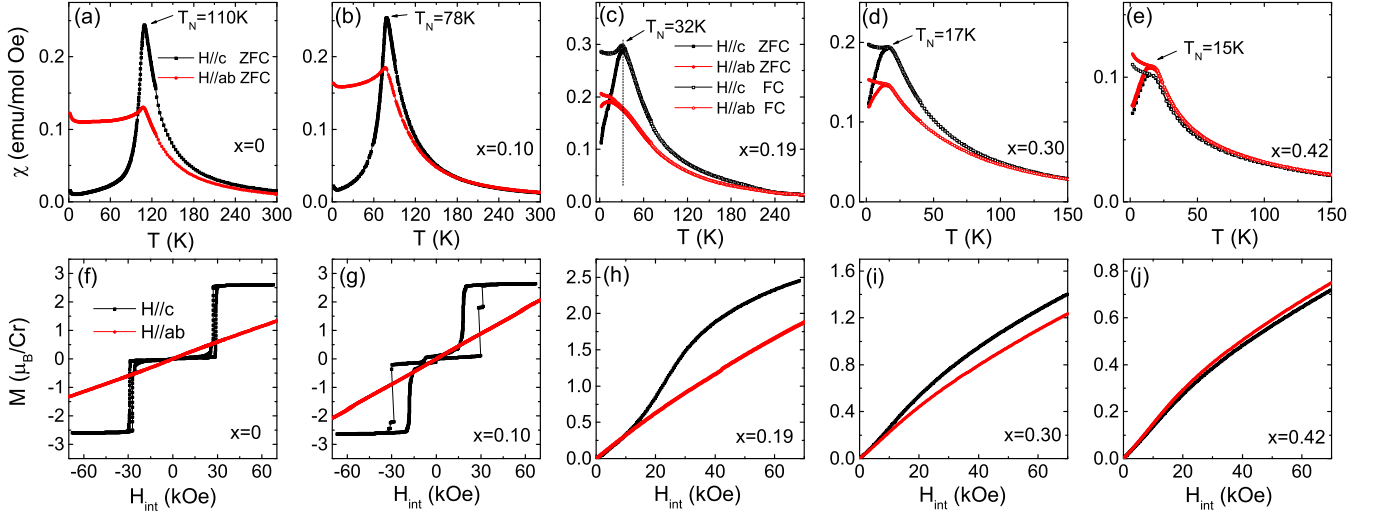


FIG. 2. (a)-(e) The temperature dependent magnetic susceptibilities measured on $\text{NaCr}(\text{Te}_{1-x}\text{Se}_x)_2$ ($0 \leq x \leq 0.42$) under magnetic field applied along ab -plane or c -axis. (f)-(j) Magnetization isotherms measured on the same crystals at $T = 2$ K. For $x = 0$ and $x = 0.10$, the hysteresis loops are presented.

axis with $(1/3 \ 1/3)$ translation in the ab -plane. So the c -lattice parameter has almost tripled. These two different structures are referred as 'Te-phase' and 'Se-phase' respectively in the following descriptions.

For $\text{NaCr}(\text{Te}_{1-x}\text{Se}_x)_2$ ($0 \leq x \leq 1$), the lattice parameters were obtained by refining the single crystal x-ray diffraction data and plotted in Fig. 1(c) and (d). The results show that the samples with $x \leq 0.5$ maintain the Te-phase while the samples with $x \geq 0.68$ are confirmed to have the Se-phase. Therefore the phase boundary may exist near $x = 0.6$, although it has not been accurately determined. The precession images from the single crystal x-ray diffraction data display streaking features for most doped samples, especially for the heavily doped ones. This indicates that notable stacking disorders and possible phase separations may exist in $\text{NaCr}(\text{Te}_{1-x}\text{Se}_x)_2$ (Figure S2 in Supplementary Materials[26]). In the Te-phase zone, both the a - and c -lattice parameters do not follow a monotonic change with increasing x . Compare with NaCrTe_2 , there is a 7% shrinkage for the a -axis of NaCrSe_2 . The c -lattice parameter for NaCrS_2 is 19.485 \AA , which decreases about 4% compared with that of NaCrSe_2 .

Previous calculations of the cleavage energies suggest that NaCrX_2 can be exfoliated to a thickness of a few layers[18]. We performed the mechanical exfoliation of bulk NaCrX_2 single crystals using Scotch tape. Nanosheets of NaCrTe_2 and NaCrSe_2 with thickness 20-30 nm could be obtained, which is demonstrated by the atomic force microscopy images in Fig. 1(e) and (f). Recently Jing Peng *et al.* demonstrated that isostructural AgCrS_2 can be exfoliated into 1.1 nm nanosheet which consists of one Ag-layer sandwiched between two CrS_2 -layers[17]. Therefore this class of materials are promising

2D materials for further investigations. Future investigation on whether NaCrX_2 is stable under similar exfoliation method as AgCrS_2 could be stimulated.

Magnetic properties of $\text{NaCr}(\text{Te}_{1-x}\text{Se}_x)_2$

The temperature dependent magnetic susceptibility $\chi(T)$ and isothermal magnetization $M(H)$ of $\text{NaCr}(\text{Te}_{1-x}\text{Se}_x)_2$ single crystals are shown in Fig. 2. Demagnetization corrections with methods used in our previous publication have been applied on the $H \parallel c$ data and the applied magnetic field H_{app} in $M(H)$ curve is replaced by the internal field H_{int} [24]. For NaCrTe_2 , $\chi(T)$ curve under $H \parallel c$ exhibits a sharp drop down to nearly zero below $T_N = 110$ K in contrast to the weak cusp and plateau-like feature under $H \parallel ab$. This suggests the development of an A -type antiferromagnetic order (ferromagnetic intralayer and antiferromagnetic interlayer couplings) with moment aligned along c -axis. The Curie-Weiss fit on the high-temperature paramagnetic susceptibility reveals $\mu_{\text{eff}}/Cr = 3.8 \mu_B$ and $\theta_{CW} = 155$ K. The large positive θ_{CW} value indicates the strong intralayer ferromagnetic correlations. The hysteresis loops at 2 K under $H \parallel c$ and $H \parallel ab$ demonstrate the strong perpendicular magnetic anisotropy (PMA) and a spin-flip transition to the ferromagnetic state near $H_{ab} = 30$ kOe. These observations are similar as previous report[20]. The saturation moment for NaCrTe_2 is $2.6 \mu_B/Cr$, which is a bit lower than the theoretical value $3.0 \mu_B$ for Cr^{3+} in a localized model.

For $x = 0.1$, T_N decreases to 78 K while the features of A -type antiferromagnetic order and perpendicular magnetic anisotropy still persist. The spin-flip transition near

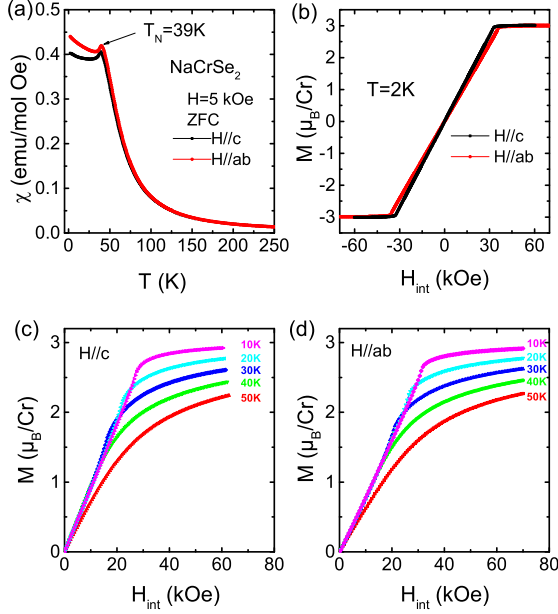


FIG. 3. Anisotropic magnetization data for NaCrSe₂ single crystal: (a) The temperature dependent magnetic susceptibilities at $H=5$ kOe. (b) Magnetic hysteresis loops at $T=2$ K. (c) and (d) Magnetization isotherms measured at selected temperatures under $H \parallel c$ and $H \parallel ab$, respectively.

30 kOe also exists but with a much larger hysteresis comparing with that of $x=0$. An important modification of magnetic anisotropy is that the PMA seems to get weakened with Se-doping. If we choose the ratio M_c/M_{ab} at $H=60$ kOe and $T=2$ K as a criterion, it decreases from 2.3 for $x=0$ to 1.5 for $x=0.10$.

With increasing doping concentration x , T_N continuously shifts to lower temperature and the spin-flip transition gradually vanishes as shown in Fig. 2(c)-(d) and (h)-(j). The M_c/M_{ab} at 60 kOe and 2 K also gradually decreases from 1.4 ($x=0.19$) to 1.2 ($x=0.30$), and finally to 0.95 ($x=0.42$). This means the magnetic anisotropy gradually evolves from PMA to a slightly preferred in-plane magnetization. On the other hand, for $x \geq 0.19$, there is a bifurcation between zero-field-cooling (ZFC) and field-cooling (FC) magnetization below T_N , which implies the emergence of a spin-glass state. In addition, the Curie-Weiss fit on the doped samples reveals similar values of effective moment but lower θ_{CW} values (131 K-106 K), suggest a slightly weakened ferromagnetic correlations.

The samples with $0 \leq x \leq 0.42$ discussed above all belongs to the Te-phase. Our XRD analysis reveal that at least from $x=0.68$, NaCr(Te_{1-x}Se_x)₂ enters the Se-phase. Let us first discuss the magnetic properties of NaCrSe₂ which is shown in Fig. 3. A cusp at $T_N=39$ K is observed in the $\chi(T)$ curve indicating an antiferromagnetic transition. On the other hand, fitting the high-

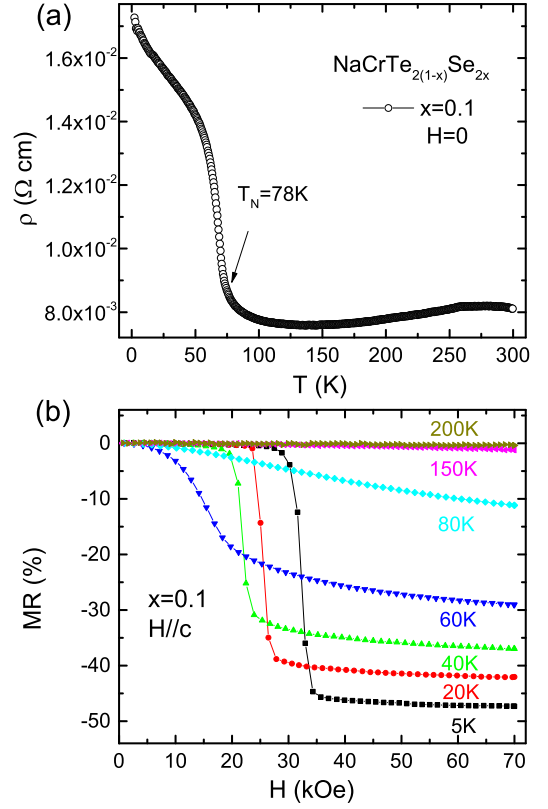


FIG. 4. (a) The temperature dependent resistivity of NaCr(Te_{1-x}Se_x)₂ with $x=0.1$ under zero field. (b) Isothermal magnetoresistance (MR) of $x=0.1$ under $H \parallel c$.

temperature paramagnetic data to the Curie-Weiss law yields $\mu_{eff}/Cr = 3.8 \mu_B$ and $\theta_{CW} = 108$ K. The positive θ_{CW} temperature indicates ferromagnetic correlations are still strong in each individual layer, while the interlayer coupling is antiferromagnetic, similar as NaCrTe₂ and many other 2D layered magnetic materials.

In contrast to the strong anisotropic magnetization under $H \parallel c$ and $H \parallel ab$ for NaCrTe₂, the magnetic anisotropy of NaCrSe₂ is much smaller. Without applying a demagnetization correction, NaCrSe₂ appears to have essentially zero anisotropy. After the correction, a weak PMA could be identified from the $M(H)$ curves at 2 K [Fig. 3(b)]. Under $H \geq 30$ kOe for both directions and $T=2$ K, the magnetization becomes saturated with a saturation moment of $3.0 \mu_B/Cr$, which is larger than that of NaCrTe₂ and accurately equals to the theoretical value of Cr³⁺ in a localized model. It should be noted that, before reaching saturated value, the magnetization increases quickly and linearly with increasing field along both directions. This indicate that although the spins of NaCrSe₂ are antiferromagnetically aligned at low field, they could be continuously canted along the field direction with increasing field. Fig. 3(c) and (d) show the $M(H)$ curves at different temperatures. The satura-

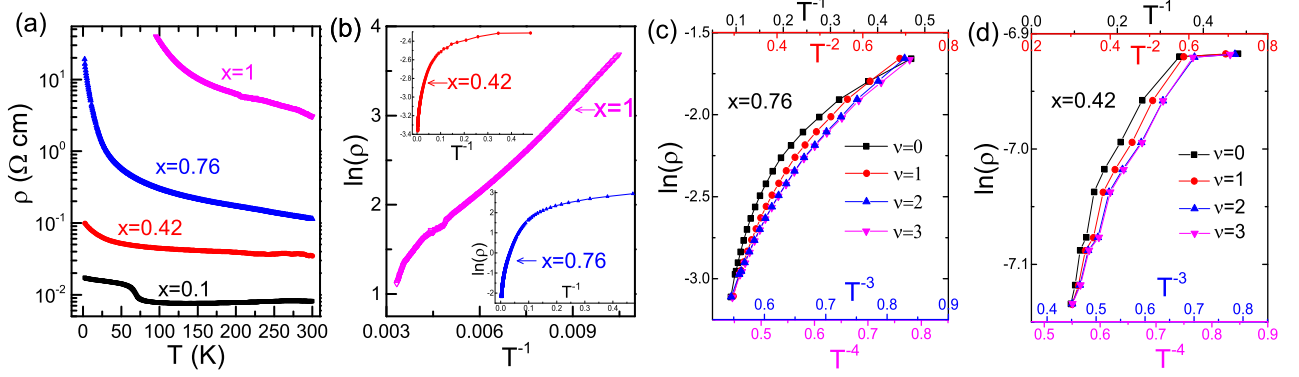


FIG. 5. (a) Temperature dependent resistivity data for $\text{NaCr}(\text{Te}_{1-x}\text{Se}_x)_2$ ($H=0$). (b) $\ln \rho$ versus T^{-1} plot of $x=1$ for all measured temperatures. The inset shows same plots for $x=0.42$ and $x=0.76$. (c,d) Low temperature $\ln \rho$ versus $T^{-1/(\nu+1)}$ plots of $x=0.76$ and $x=0.42$, respectively. ν is the parameter from VRH formula.

tion moment gradually decreases with increasing temperature. At 50 K which is well above T_N , the $M(H)$ curve still exhibits a nonlinear curvature and a large moment ($\sim 2.2 \mu_B/\text{Cr}$) at 60 kOe. In addition, the $M(T)$ curve also deviates from Curie-Weiss behavior below 200 K, which are actually observed for all NaCrX_2 ($X=\text{Te, Se, S}$) samples. These observations suggests that strong magnetic fluctuations or short-range magnetic order may develop well above T_N .

For $x=0.68$ and $x=0.79$ with Se-phase, the spin-glass behavior are quite similar as $x=0.42$ with Te-phase. The related magnetization data is not shown here but the results are plotted in the phase diagram of Fig. 6. Further discussions about the evolution of anisotropic magnetic properties of $\text{NaCr}(\text{Te}_{1-x}\text{Se}_x)_2$ will be presented in the following section with the phase diagram.

Tunable conductivity in $\text{NaCr}(\text{Te}_{1-x}\text{Se}_x)_2$

Previously, NaCrTe_2 was reported to exhibit a metal-insulator-like transition due to the formation of A -type antiferromagnetic ordering[20]. Similarly, the resistivity of $x=0.1$ sample has a typical metallic behavior above 130 K [Fig. 4(a)], while a sharp jump appears at $T_N=78$ K with decreasing temperature which should result from the localization of charge carriers by long-range antiferromagnetic order. With further decreasing temperature, the resistivity continues to increase with a smaller slope which might be attributed to the impurity scattering effect by chemical-doping. Under magnetic field along c -axis, a giant negative magnetoresistance appears with maximal value up to 48% at 5 K and 70 kOe. This behavior is directly associated with the field-induced spin-flip transition and due to the reduced spin scattering to the electrons in the ferromagnetic state comparing with that in the antiferromagnetic states.

Comparing with the previously reported resistivity of NaCrTe_2 [20], we noticed that the value for $x=0.1$ approximately increases by an order of magnitude. As shown in Fig. 5(a), intriguingly, with further increasing Se-doping concentration x , the temperature dependent resistivity of $\text{NaCr}(\text{Te}_{1-x}\text{Se}_x)_2$ becomes fully semiconducting-like and the absolute value of resistivity continuously increases by several orders. For NaCrSe_2 with $x=1$, the resistivity is about $\sim 10 \Omega \cdot \text{cm}$ and the data below 95 K cannot be obtained due to the upper limit of PPMS measurement. Thus a Se-doping induced metal-insulator transition is observed for $\text{NaCr}(\text{Te}_{1-x}\text{Se}_x)_2$.

Density functional theory calculations have shown that both NaCrTe_2 and NaCrSe_2 are semiconductors, their band gaps are 0.59 eV and 0.77 eV respectively[18]. In order to check whether the doping controlled conductivity is due to the gradual increasing of the band gap, we have tried to fit the resistivity data using the thermal activation model as described by $\rho=\rho_0\exp(E_a/2k_B T)$. Where E_a is the energy gap and k_B is the Boltzmann constant. Therefore a fine fitting result using this formula can only be obtained when $\ln \rho$ and T^{-1} follows a linear relationship. However, as shown in Fig. 5(b), there are not well defined linear relations between $\ln \rho$ and T^{-1} for all samples, especially for $x=0.42$ and $x=0.76$.

For chemical doped samples, the doping-induced strong disorder potential might trap itinerant electrons and lead to a metal-insulator transition, which is the famous Anderson localization[27]. For an Anderson insulator at low temperatures, there are electronic states trapped in the vicinity of the Fermi surface and the hopping transport by localized electrons would be described by the variable range hopping (VRH) model $\rho=\rho_0\exp(T_0/T)^{1/(\nu+1)}$ [28]. In this formula, $\nu=0$ denotes the traditional insulator with band gap (same as thermal activation model described above). $\nu=1, 2$ and 3 correspond to one-, two-, and three-dimensional material

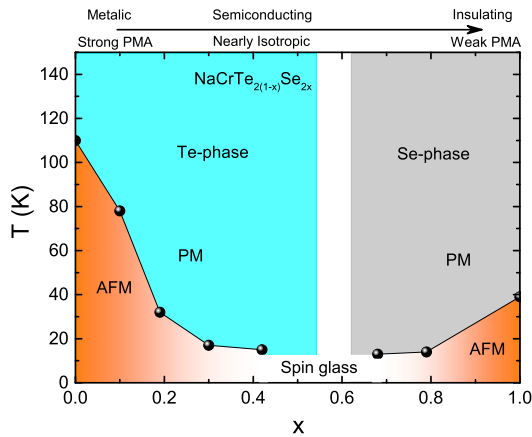


FIG. 6. Temperature versus doping phase diagram for $\text{NaCr}(\text{Te}_{1-x}\text{Se}_x)_2$ ($0 \leq x \leq 1$).

with Anderson localization, respectively. In Fig. 5(c) and (d), the $\ln \rho$ versus $T^{-1/(\nu+1)}$ plots for $x=0.42$ and 0.76 from 2 K to 10 K are presented. Although a perfect straight line is not observed, the formula using $\nu=2$ or $\nu=3$ would clearly give a much better fitting results comparing with that using $\nu=0$, especially for $x=0.76$. Our results indicate that the significant enhancement of resistivity in $\text{NaCr}(\text{Te}_{1-x}\text{Se}_x)_2$ may partially originate from the Anderson localization. Besides, the tuning of band gap by Se-doping would also be possible. The electronic transport properties of $\text{NaCr}(\text{Te}_{1-x}\text{Se}_x)_2$ may contains contributions from these two aspects.

Discussion on the phase diagram of $\text{NaCr}(\text{Te}_{1-x}\text{Se}_x)_2$

The T - x phase diagram of $\text{NaCr}(\text{Te}_{1-x}\text{Se}_x)_2$ is presented in Fig. 6, which summarizes the major experimental results above. Three features should be mentioned about this phase diagram. Firstly, considering either from Se-doped NaCrTe_2 or Te-doped NaCrSe_2 , the antiferromagnetic transition temperature gradually decreases and the system enters a spin-glass state with increasing doping concentration. Secondly, the magnetic anisotropy can be effectively tuned by chemical doping in this system. NaCrTe_2 possesses a strong PMA and it continuously gets weakened and evolves into a nearly isotropic magnetic behavior at $x=0.42$ while maintain the Te-phase. For NaCrSe_2 at the other end, a weak PMA is identified. Thirdly, A systematic change in the conductivity of $\text{NaCr}(\text{Te}_{1-x}\text{Se}_x)_2$ occurs on increasing x , from bad metallic behavior in NaCrTe_2 to the semiconducting or insulating behavior in NaCrSe_2 .

The doping-induced disorder effect and stacking faults should be responsible for the emergence of the spin glass state[29]. It also may play an important role in tuning the magnetic anisotropy in $\text{NaCr}(\text{Te}_{1-x}\text{Se}_x)_2$. In previous investigations on materials for high-density mag-

netic recording media, chemical disorder has been shown to have important influence on the magnetocrystalline anisotropy energy (MAE)[30–32]. It may either drastically reduce the MAE or tune the MAE to a maximum value[30–32]. For vdW material, recent studies reveal that $\text{Ni}_{1-x}\text{Fe}_x\text{PS}_3$ and $\text{Fe}_{5(1-x)}\text{Co}_{5x}\text{GeTe}_2$ enable chemical tuning of easy-plane and easy-axis anisotropies[24, 25, 33]. Magnetic anisotropy is a key property of 2D magnets, which is required for counteracting thermal fluctuations. There have been reports about pressure control of magnetic anisotropy on CrGeTe_6 [34] and tensile strain-tunable magnetic anisotropy in monolayer CrX_3 ($x=\text{Cl, Br, I}$)[35]. Our study provides a new example for chemical disorder or stacking fault controlled magnetic anisotropy in 2D magnetic material $\text{NaCr}(\text{Te}_{1-x}\text{Se}_x)_2$.

In addition, one should notice that the magnetic anisotropy also makes a big difference between NaCrTe_2 and NaCrSe_2 , both of them seem to have no evident chemical disorder. A possible speculation is that, for NaCrSe_2 with relatively much lighter Se element, the spin-orbit coupling effect may become weak and results in a weak PMA[36]. As we mentioned above, the saturation moment of NaCrSe_2 agrees well with the expectation of Cr^{3+} spin $S=3/2$ model without orbital moment while that of NaCrTe_2 has a notable smaller value which might be due to the enhanced spin-orbital coupling.

The tuning of conductivity by chemical doping in 2D magnetic material has been rarely reported. This effect found in $\text{NaCr}(\text{Te}_{1-x}\text{Se}_x)_2$, possibly due to Anderson localization and the change of band structure, may have important applications in designing novel spintronic devices. Particularly, the chemical doping in $\text{NaCr}(\text{Te}_{1-x}\text{Se}_x)_2$ could simultaneously tune both the conductivity and magnetic anisotropy.

Field-induced metamagnetic transitions in NaCrS_2

For the magnetic properties of NaCrS_2 , so far as we know, there has not been any investigations on the single crystals. We present the anisotropic magnetization data on NaCrS_2 single crystals in Fig. 7. The different temperature dependent features of χ_{ab} and χ_c below $T_N=19$ K indicate the ordered magnetic moment should be confined within ab -plane [Fig. 7(a)]. Fig. 7(b) present the magnetic hysteresis loops at 2 K. Under magnetic field applied along the hard-axis ($H \parallel c$), a linear relationship between magnetization and field is observed. But for field applied along the easy ab -plane, a sudden magnetization jump is revealed at around 25 kOe suggest the occurrence of field-induced metamagnetic transition. From the magnetization isotherms at higher temperatures [Fig. 7 (c) and (d)], the linear behavior persists for $H \parallel c$ and the magnetization jump gradually weakens with increasing temperature for $H \parallel ab$. The contour

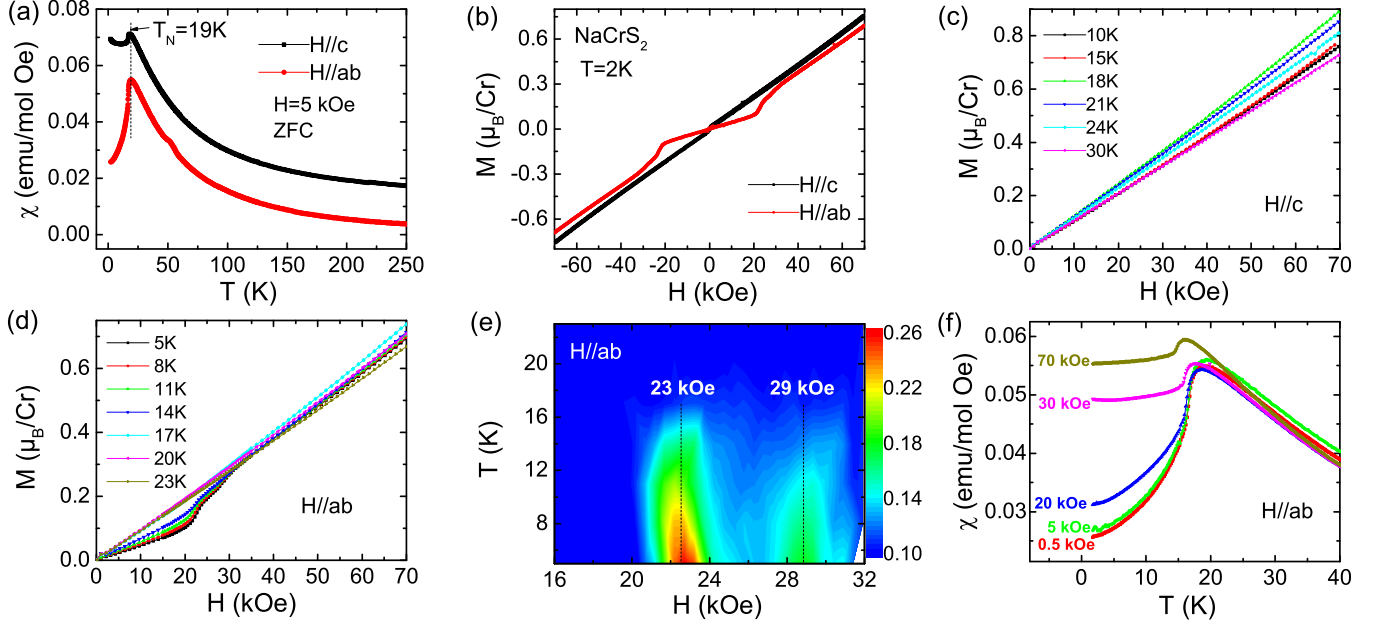


FIG. 7. Anisotropic magnetization data for NaCrS₂ single crystal: (a) The temperature dependent magnetic susceptibilities at $H=5$ kOe. (b) Magnetic hysteresis loops at $T=2$ K. (c) and (d) Magnetization isotherms measured at selected temperatures under $H \parallel c$ and $H \parallel ab$, respectively. (e) Contour plot of dM/dH as a function of temperature and field along $H \parallel ab$. (f) The temperature dependent magnetic susceptibilities under different applied field near the antiferromagnetic transition.

plot of dM_{ab}/dH in Fig. 7(e) reveals that there are actually two metamagnetic transitions which appear at $H=23$ kOe and $H=29$ kOe respectively. These two transitions gradually disappear near T_N . The transition at lower field slightly softens with increasing temperature similar as that for a conventional spin-flip transition.

Early neutron diffraction result on NaCrS₂ powders have determined its magnetic structure to be a in-plane helical one[21]. The spins of Cr have antiferromagnetic coupling along the c -axis, while in the ab -plane they are aligned in a helimagnetic order with rotating angle $\phi = 33^\circ$ in adjacent (110) planes[21]. This ground state magnetic structure is consistent with the anisotropic magnetic behavior of our single-crystal sample. It is interesting to point out that the Curie-Weiss fit gives still positive θ_{CW} values (18 K for $H \parallel ab$ and 31 K for $H \parallel c$) which suggests the ferromagnetic correlations still exist. In addition, we noticed that the paramagnetic susceptibility and corresponding fitted θ_{CW} values have large anisotropy. Whether this really means the anisotropy on the exchange interactions need further researches to clarify, as this kind of difference can arise solely from the single-ion anisotropy even without exchange interaction as in a previous theoretical research[37].

Furthermore, the observed field-induced metamagnetic transitions should have significant influences on this complex helimagnetic order. Firstly, the magnetic order under field above 30 kOe should also be antiferromagnetic-like. This is supported by the cusp-like feature in the $\chi_{ab} - T$ curve at T_N , as shown in Fig. 7 (f). The an-

tiferromagnetic transition seems to be quite robust under field. T_N only has a slight shift to 16 K under $H = 70$ kOe. In addition, $M(H)$ curve follows a linear relationship up to 70 kOe with a small value of moment ($\sim 0.7\mu_B/\text{Cr}$) under this field. Secondly, for $H_{ab} \leq 20$ kOe the magnetic susceptibilities have a sharp drop below T_N . In contrast, for $H_{ab} = 30$ kOe and 70 kOe, the magnetic susceptibilities exhibit a plateau below T_N , which is a typical feature of canted antiferromagnetic magnetic order. Therefore, new types of antiferromagnetic order are expected under in-plane magnetic field, which would be an interesting topic for further investigations using neutron scattering.

CONCLUSIONS

In summary, the physical properties of NaCrX₂ (X=Te,Se,S) are investigated in single-crystal form. For NaCr(Te_{1-x}Se_x)₂, a field-induced spin-flip transition together with a giant negative magnetoresistance are observed at $x \leq 0.1$. At higher doping level, a spin glass state emerges. The most prominent feature is that both the magnetic anisotropy and the conductivity can be effectively tuned by x . For NaCrS₂, two magnetic field induced metamagnetic transitions are identified. We further demonstrate that these crystals can be mechanically-exfoliated into nano-flakes. These properties would make NaCrX₂ a promising material playground for further investigations on 2D magnetism and designing novel

magneto-electronic devices. Furthermore, our samples also provide a route to vdW layered CrX_2 through deintercalation.

ACKNOWLEDGEMENT

This work was supported by the National Natural Science Foundation of China (No. 12074426, No. 11227906 and No. 12004426), the Fundamental Research Funds for the Central Universities, and the Research Funds of Renmin University of China (Grants No. 22XNKJ40).

* Corresponding author: pcheng@ruc.edu.cn

- [1] K. S. Burch, D. Mandrus, and J.-G. Park, *Nature* **563**, 47 (2018).
- [2] H. Li, S. Ruan, and Y.-J. Zeng, *Advanced Materials* **31**, 1900065 (2019).
- [3] D. L. Cortie, G. L. Causer, K. C. Rule, H. Fritzsche, W. Kreuzpaintner, and F. Klose, *Advanced Functional Materials* **30**, 1901414 (2020).
- [4] Y. Deng, Y. Yu, Y. Song, J. Zhang, N. Z. Wang, Z. Sun, Y. Yi, Y. Z. Wu, S. Wu, J. Zhu, J. Wang, X. H. Chen, and Y. Zhang, *Nature* **563**, 94 (2018).
- [5] Z. Fei, B. Huang, P. Malinowski, W. Wang, T. Song, J. Sanchez, W. Yao, D. Xiao, X. Zhu, A. F. May, W. Wu, D. H. Cobden, J.-H. Chu, and X. Xu, *Nature Materials* **17**, 778 (2018).
- [6] B. Huang, G. Clark, E. Navarromoratalla, D. R. Klein, R. Cheng, K. L. Seyler, D. Zhong, E. Schmidgall, M. A. McGuire, and D. H. Cobden, *Nature* **546**, 270 (2017).
- [7] C. Gong, L. Li, Z. Li, H. Ji, A. Stern, Y. Xia, T. Cao, W. Bao, C. Wang, and Y. Wang, *Nature* **546**, 265 (2017).
- [8] J.-U. Lee, S. Lee, J. H. Ryoo, S. Kang, T. Y. Kim, P. Kim, C.-H. Park, J.-G. Park, and H. Cheong, *Nano Letters* **16**, 7433 (2016).
- [9] X. Wang, K. Du, Y. Y. F. Liu, P. Hu, J. Zhang, Q. Zhang, M. H. S. Owen, X. Lu, C. K. Gan, P. Sengupta, C. Kloc, and Q. Xiong, *2D Materials* **3**, 031009 (2016).
- [10] D. C. Freitas, R. Weht, A. Sulpice, G. Remenyi, P. Strobel, F. Gay, J. Marcus, and M. Núñez-Regueiro, *Journal of Physics: Condensed Matter* **27**, 176002 (2015).
- [11] X. Sun, W. Li, X. Wang, Q. Sui, T. Zhang, Z. Wang, L. Liu, D. Li, S. Feng, S. Zhong, H. Wang, V. Bouchiat, M. Nunez Regueiro, N. Rougemaille, J. Coraux, A. Purbawati, A. Hadj-Azzem, Z. Wang, B. Dong, X. Wu, T. Yang, G. Yu, B. Wang, Z. Han, X. Han, and Z. Zhang, *Nano Research* **13**, 3358 (2020).
- [12] X. Zhang, Q. Lu, W. Liu, W. Niu, J. Sun, J. Cook, M. Vaninger, P. F. Miceli, D. J. Singh, S.-W. Lian, T.-R. Chang, X. He, J. Du, L. He, R. Zhang, G. Bian, and Y. Xu, *Nature Communications* **12**, 2492 (2021).
- [13] L. Meng, Z. Zhou, M. Xu, S. Yang, K. Si, L. Liu, X. Wang, H. Jiang, B. Li, P. Qin, P. Zhang, J. Wang, Z. Liu, P. Tang, Y. Ye, W. Zhou, L. Bao, H.-J. Gao, and Y. Gong, *Nature Communications* **12**, 809 (2021).
- [14] F. Fabre, A. Finco, A. Purbawati, A. Hadj-Azzem, N. Rougemaille, J. Coraux, I. Philip, and V. Jacques, *Phys. Rev. Materials* **5**, 034008 (2021).
- [15] J.-J. Xian, C. Wang, J.-H. Nie, R. Li, M. Han, J. Lin, W.-H. Zhang, Z.-Y. Liu, Z.-M. Zhang, M.-P. Miao, Y. Yi, S. Wu, X. Chen, J. Han, Z. Xia, W. Ji, and Y.-S. Fu, *Nature Communications* **13**, 257 (2022).
- [16] M. Huang, Z. Ma, S. Wang, S. Li, M. Li, J. Xiang, P. Liu, G. Hu, Z. Zhang, Z. Sun, Y. Lu, Z. Sheng, G. Chen, Y.-L. Chueh, S. A. Yang, and B. Xiang, *2D Materials* **8**, 031003 (2021).
- [17] J. Peng, Y. Liu, H. Lv, Y. Li, Y. Lin, Y. Su, J. Wu, H. Liu, Y. Guo, Z. Zhuo, X. Wu, C. Wu, and Y. Xie, *Nature Chemistry* **13**, 1235 (2021).
- [18] W. Xu, S. Ali, Y. Jin, X. Wu, and H. Xu, *ACS Applied Electronic Materials* **2**, 3853 (2020).
- [19] S. Kobayashi, H. Ueda, C. Michioka, and K. Yoshimura, *Inorganic Chemistry* **55**, 7407 (2016).
- [20] J. Wang, J. Deng, X. Liang, G. Gao, T. Ying, S. Tian, H. Lei, Y. Song, X. Chen, J.-g. Guo, and X. Chen, *Phys. Rev. Materials* **5**, L091401 (2021).
- [21] F. Engelsman, G. Wieggers, F. Jellinek, and B. Van Laar, *Journal of Solid State Chemistry* **6**, 574 (1973).
- [22] C.-K. Tian, C. Wang, W. Ji, J.-C. Wang, T.-L. Xia, L. Wang, J.-J. Liu, H.-X. Zhang, and P. Cheng, *Phys. Rev. B* **99**, 184428 (2019).
- [23] J. Sheng, X. Li, C. Tian, J. Song, X. Li, G. Sun, T. Xia, J. Wang, J. Liu, D. Xu, H. Zhang, X. Tong, W. Luo, L. Wu, W. Bao, and P. Cheng, *Phys. Rev. B* **101**, 174516 (2020).
- [24] C. Tian, F. Pan, S. Xu, K. Ai, T. Xia, and P. Cheng, *Applied Physics Letters* **116**, 202402 (2020).
- [25] S. Lee, J. Park, Y. Choi, K. Raju, W.-T. Chen, R. Sankar, and K.-Y. Choi, *Phys. Rev. B* **104**, 174412 (2021).
- [26] See Supplemental Material at [URL will be inserted by publisher] for details about structural and composition analysis of $\text{NaCr}(\text{Te}_{1-x}\text{Se}_x)_2$ through single-crystal x-ray diffraction and EDS..
- [27] P. W. Anderson, *Phys. Rev.* **109**, 1492 (1958).
- [28] T. Ying, Y. Gu, X. Chen, X. Wang, S. Jin, L. Zhao, W. Zhang, and X. Chen, *Science Advances* **2**, e1501283 (2016).
- [29] K. Binder and A. P. Young, *Rev. Mod. Phys.* **58**, 801 (1986).
- [30] C. J. Aas, L. Szunyogh, J. S. Chen, and R. W. Chantrell, *Applied Physics Letters* **99**, 132501 (2011).
- [31] M. Si, A. Izardar, and C. Ederer, *arXiv:2111.12492* (2021).
- [32] C. Neise, S. Schonecker, M. Richter, K. Koepf, and H. Eschrig, *physica status solidi (b)* **248**, 2398 (2011).
- [33] A. F. May, M.-H. Du, V. R. Cooper, and M. A. McGuire, *Phys. Rev. Materials* **4**, 074008 (2020).
- [34] T. Sakurai, B. Rubrecht, L. T. Corredor, R. Takehara, M. Yasutani, J. Zeisner, A. Alfonsov, S. Selter, S. Aswartham, A. U. B. Wolter, B. Büchner, H. Ohta, and V. Kataev, *Phys. Rev. B* **103**, 024404 (2021).
- [35] L. Webster and J.-A. Yan, *Phys. Rev. B* **98**, 144411 (2018).
- [36] F. Xue, Y. Hou, Z. Wang, and R. Wu, *Phys. Rev. B* **100**, 224429 (2019).
- [37] D. C. Johnston, *Phys. Rev. B* **95**, 094421 (2017).